Measurement of $H\to\mu^+\mu^-$ production in association with a Z boson at the CEPC*

Zhen-Wei Cui(崔震崴)[1;1)] Qiang Li(李强)[1,2;2)] Gang Li(李刚)[2,3] Man-Qi Ruan(阮曼奇)[2,3]
Lei Wang(王磊)[1] Da-Neng Yang(杨大能)[1]

[1] Department of Physics and State Key Laboratory of Nuclear Physics and Technology, Peking University, Beijing 100871, China
[2] CAS Center for Excellence in Particle Physics, Beijing 100049, China
[3] Institute of High Energy Physics, Beijing 100049, China

Abstract: The Circular Electron-Positron Collider (CEPC) is a future Higgs factory proposed by the Chinese high energy physics community. It is planned to operate at a center-of-mass energy of 240–250 GeV and is expected to accumulate an integrated luminosity of 5 ab^{-1} over ten years of operation. At the CEPC, Higgs bosons will be dominantly produced from the ZH associated process. The vast number of Higgs events collected will enable precise studies of its properties, including Yukawa couplings to massive particles. With GEANT4-based simulation of detector effects, we study the feasibility of measuring the Higgs boson decaying into a pair of muons at the CEPC. The results with and without information from the Z boson decay products are provided, showing that a signal significance of over 10 standard deviations can be achieved and the H-μ-μ coupling can be measured within 10% accuracy.

Keywords: Higgs, CEPC, Yukawa coupling

PACS: 13.66.Fg, 14.80.Bn, 13.66.Jn **DOI:** 10.1088/1674-1137/42/5/053001

1 Introduction

The discovery of the Higgs-like boson completes the particle table of the Standard Model (SM) of particle physics. Up-to-date LHC measurements all indicate that the Higgs boson is indeed highly SM-like [1–6]. In the SM, Higgs couplings to massive particles are proportional to their mass (squared). Hence, the event rate of Higgs couplings to the first and second generation of massive fermions can be very small, making them difficult to measure at the LHC. The Circular Electron-Positron Collider (CEPC) [7], however, is designed to run at around 240∼250 GeV with a combined instantaneous luminosity of 2×10^{34} cm^{-2} s^{-1} for the two planned experiments, and will deliver 5 ab^{-1} of integrated luminosity over ten years of running. The huge amount of data will enable precise measurement of the branching ratios of the Higgs to light fermions and determine the associated Yukawa couplings, including H-μ-μ, which is crucial to validate the consistency of the SM Higgs mechanism, since any deviation would indicate the existence of new physics.

Searches for $H\to\mu^+\mu^-$ production have been performed at the ATLAS and CMS experiments with Run-I and Run-II data [8–10]. The most stringent observed (expected) upper limit on the cross-section times branching ratio is found to be 2.8 (2.9) times the SM prediction [10]. Projections have also been made for the High Luminosity-LHC assuming an integrated luminosity of 3000 fb^{-1} collected by the ATLAS or CMS detector, which can lead to a signal significance of about 7 σ [11] with an accuracy of around 20% [12]. Studies have also been performed for the International Linear Collider (ILC). Considering a center mass energy of 250 GeV and an integrated luminosity of 250 fb^{-1}, the signal is dominated by the Higgs-strahlung from a Z boson and the signal significances for the sub-processes with a Z boson decaying into $\nu\bar{\nu}$ and $q\bar{q}$ are found to be 1.8 and 1.1 σ, respectively [13]. Then, accumulating 2000 fb^{-1} at 250 GeV and 4000 fb^{-1} at 500 GeV with actual beam polarization, the precision of signal strength becomes 20.5% and 15.4% respectively [14]. At a center-of-mass energy of 1 TeV with an integrated luminosity of 500 fb^{-1}, the

Received 29 November 2017, Revised 12 February 2018, Published online 13 April 2018

∗ Supported by National Natural Science Foundation of China (11475190, 11575005), CAS Center for Excellence in Particle Physics (CCEPP) and CAS Hundred Talent Program (Y3515540U1)

1) E-mail: lovekey@pku.edu.cn

2) E-mail: qliphy0@pku.edu.cn

signal is dominated by the WW-fusion process and a sensitivity of 2.75 σ can be achieved [15].

At the CEPC, the signal $H \to \mu^+\mu^-$ production is dominated by the Higgs-strahlung from a Z boson. We perform a feasibility study based on events generated at leading order accuracy with initial state radiation (ISR), parton shower, hadronization and detector effects simulated.

Considering that 70% of the Z bosons decay hadronically and 20% decay invisibly, we focus on two scenarios, one for Z boson inclusive decay and the other for hadronic decay. The first case maximally exploits the statistics of the produced $H\to\mu^+\mu^-$ events and the second takes advantage of the major part of the decay kinematics. For both cases, we first perform a cut-based analysis and then improve the measurement using a Boosted Decision Tree (BDT) technique.

This paper is organized as follows. Section 2 describes event generation and simulation. Section 3 presents results for the inclusive measurement. Section 4 presents results for the $Z\to q\bar{q}$ decay channel. Section 5 summarizes the paper.

2 Monte Carlo simulation

At a 250 GeV CEPC, Higgs bosons will mainly be produced through Higgs-strahlung, i.e. $e^+e^- \to ZH$. With an integrated luminosity of 5000 fb^{-1}, about 230 of our signal events $H \to \mu^+\mu^-$ can be produced. The expected background to the signal production includes 2-fermion processes $e^+e^- \to f\bar{f}$, where f can be any SM fermion other than the top quark, and 4-fermion processes, which can be mediated through associated ZZ, WW, ZZ, WW production and a single Z boson production. All Monte Carlo (MC) events are generated with the Whizard V1.9.5 [16] event generator at parton level with ISR and interference effects included. The generated events are interfaced to Pythia 6 [17] for parton shower and hadronization simulation. Detector effects are simulated with the CEPC detector implemented with Mokka/GEANT4 [7, 18, 19]. The detector is assumed to have a similar structure to the International Large Detector (ILD) [20, 21] at the ILC [22]. At the CEPC, the muon identification efficiency is expected to be over 99.5% for P_T larger than 10 GeV, and with excellent P_T resolution of $\sigma_{1/P_T} = 2\times10^{-5}\oplus1\times10^{-3}/(P_T\sin\theta)$. The fully simulated events are reconstructed with a particle-flow algorithm ArborPFA [23]. More details about the CEPC sample set can be found in Ref. [24].

The major SM backgrounds, including all the 2-fermion processes ($e^+e^-\to f\bar{f}$, where $f\bar{f}$ refers to all lepton and quark pairs except $t\bar{t}$) and 4-fermion processes (ZZ, WW, ZZ or WW, single Z). The initial state radiation (ISR) and all possible interference effects are automatically taken into account in the generation. The classification for four fermion production follows that of LEP [25], depending crucially on the final state. For example, if the final states consist of two mutually charge conjugated fermion pairs that could decay from both WW and ZZ intermediate states, such as $e^+e^-\nu_e\bar{\nu}_e$, this is classified as a "ZZ or WW" process. If there is $e^\pm$ together with its partner neutrino and an on-shell W boson in the final state, this is called a "single W" process. Meanwhile, if there is an electron-positron pair and an on-shell Z boson in the final state, it is called a "single Z" process. Detailed information on the 2-fermion and 4-fermion samples used in our analyses are listed in Tables A1 and A2.

3 Inclusive analysis

A recoil mass method enables a measurement of the $H\to\mu^+\mu^-$ production without measuring the associated Z boson decay. We define the recoil mass as

$$M^2_{\rm recoil}=s+M^2_{\rm H}-2\cdot E_{\rm H}\cdot\sqrt{s}\ , \quad (1)$$

where $\sqrt{s}$ is the center-of-mass energy, and $M_{\rm H}$ and $E_{\rm H}$ correspond to the reconstructed mass and energy of the Higgs boson. The ZH ($H\to\mu^+\mu^-$) events form a peak in the $M_{\rm recoil}$ distribution at the Z boson mass window.

We select two muons with the largest transverse momenta and consider selections on the following kinematic variables: invariant mass of the di-muon system $M_{\mu^+\mu^-}$, recoil mass of the di-muon system $M^{\mu^+\mu^-}_{\rm recoil}$, transverse momentum of the di-muon system $P_{T_{\mu^+\mu^-}}$, third component of the di-muon momentum $P_{Z_{\mu^+\mu^-}}$, energy of di-muon system $E_{\mu^+\mu^-}$, and angular variables in the laboratory system frame $\cos\theta_{\mu^-}$, $\cos\theta_{\mu^+}$, $\cos\theta_{\mu^+\mu^-}$, $\cos\theta_{Z\mu^-}$, and $\cos\theta_{Z\mu^+}$, where θ_{μ^-},θ_{μ^+} means the polar angle of μ^-, μ^+ ; $\theta_{\mu^+\mu^-}$ means the angle between μ^- and μ^+ ; and $\theta_{Z\mu^\pm}$ represents the angle between the Z boson and muon leptons.

3.1 Cut-count analysis

The event numbers under selection flow, which are determined by maximizing $s/\sqrt{s+b}$, with s and b represent signal and background yields, are summarized in Table 1. The two mass windows $M_{\mu^+\mu^-}$ and $M^{\mu^+\mu^-}_{\rm recoil}$ are set in accordance with the signal signature. $P_{T_{\mu^+\mu^-}}$ and $P_{Z_{\mu^+\mu^-}}$ are set to reduce the ZZ events, where one of the Z bosons decays to $\mu^+\mu^-$, and Drell-Yan $Z\to\mu^+\mu^-$ background. The Higgs and Z boson decays can lead to different $\cos\theta_{\mu^+}$ and $\cos\theta_{\mu^-}$ distributions due to the spin-dependence of the couplings and the parity violation of the weak interaction. $\cos\theta_{\mu^+\mu^-}$ selection is chosen to supress the 2f background.

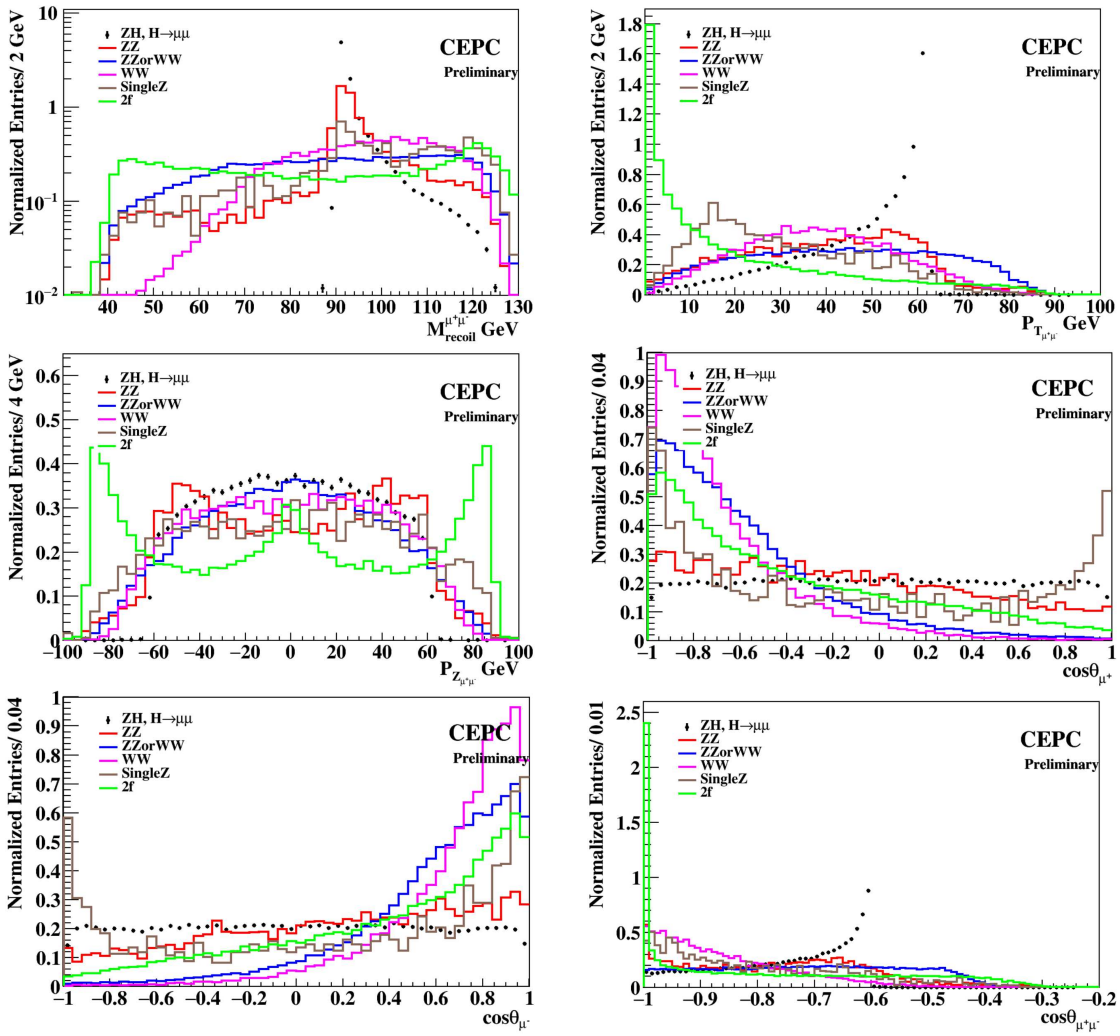

Fig. 1. (color online) Distributions of $M^{\mu^+\mu^-}_{\rm recoil}$, $P_{\rm T_{\mu^+\mu^-}}$, $P_{\rm Z_{\mu^+\mu^-}}$, $\cos\theta_{\mu^+}$, $\cos\theta_{\mu^-}$, and $\cos\theta_{\mu^+\mu^-}$ in the inclusive analysis, after the preselection (2 well identified muons) and $120<M_{\mu^+\mu^-}<130$ GeV requirements. All the distributions are normalized to 10.

Table 1. Signal and background numbers of events under selection flow for the inclusive analysis. The simulation corresponds to CEPC at $\sqrt{s}$=250 GeV with an integrated luminosity of 5000 fb^{-1}.

category	signal	ZZ	WW	ZZ or WW	single Z	2f
preselection	207.3	311312	129869	501590	63658	1740371
$120<M_{\mu^+\mu^-}<130$	189.7	5479	17126	57405	1868	52525
$90.8<M^{\mu^+\mu^-}_{\rm recoil}<93.4$	118.4	1207	868	2115	164	1157
$25<P_{\rm T_{\mu^+\mu^-}}<64$	109.8	1009	725	1772	126	452
$-56<P_{\rm Z_{\mu^+\mu^-}}<56$	107.1	969	687	1726	120	420
$\cos\theta_{\mu^-}<0.38$ $\cos\theta_{\mu^+}>-0.38$	65.2	464	49	196	53	159
$\cos\theta_{\mu^+\mu^-}>-0.996$	65.0	462	46	196	52	99
efficiency	31.3%					

An unbinned maximum likelihood fit is performed on the $M_{\mu^+\mu^-}$ distribution. The signal is parameterized by a crystal ball function, with parameters fixed by simulated events. The background is parametrized by a second order Chebychev function chosen by F-test [28].

Figure 2 shows the post-fit result of the invariant mass distribution of the di-muon system. The fitted number of signal events is 77.2±13.0. At 68% confidence

level, an accuracy from −17% to 18% can be achieved for the signal strength based on a likelihood scan. The signal under the peak at 124.4–125.2 GeV leads to a high significance of 8.8 σ, via simple couting $\sqrt{2(s+b)\ln(1+\frac{s}{b})-s}$.

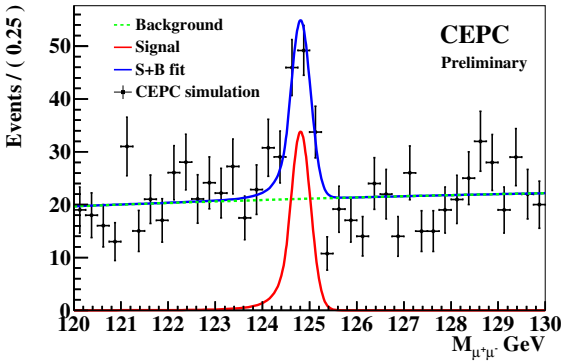

Fig. 2. (color online) The invariant mass spectrum of the di-muon system in the inclusive analysis. The dotted points with error bars represent data from the CEPC simulation.The solid red and dashed green lines correspond to the signal and background contributions respectively and the solid blue line represents the post-fit value of the total yield.

3.2 BDT optimization

We have also exploited the Toolkit for Multivariate Analysis (TMVA) [26] for further background rejection, using the method of Gradient Boosted Decision Trees (BDTG). After fixing the range of the invariant mass and the recoil mass as mentioned above, 5 variables are taken as inputs to TMVA, including $\cos\theta_{\mu^\pm Z}$, $\cos\theta_{\mu^\pm}$ and $P_{Z_{\mu^+\mu^-}}$. The choice of these variables is based on many tests and importance ranking. The resulted BDT response distribution can be seen in Figure 3, where the agreement between training and testing samples shows no obvious overtraining. We then take the final event selections as: BDTG response > 0.369, 20<$P_{T_{\mu^+\mu^-}}$<64 GeV and $\cos\theta_{\mu^+\mu^-} > -0.996$. A maximum likelihood fit is performed on the resulting invariant mass of the di-muon system. The signal and background probability functions are parametrized in the same form as in the previous cut-count study.

Figure 3 shows the BDT response distribution and the post-fit result of $M_{\mu^+\mu^-}$. The fitted number of signal events is 62.3±10.9. At 68% confidence level, an accuracy from -16% to 17% can be achieved for the signal strength based on a likelihood scan. The signal under the peak at 124.4–125.2 GeV leads to a significance of 10.9 σ.

4 Z(qq̄)H(μμ) analysis

Of all the Z boson decay modes, the hadronic channel is most promising, due to its large branching fraction

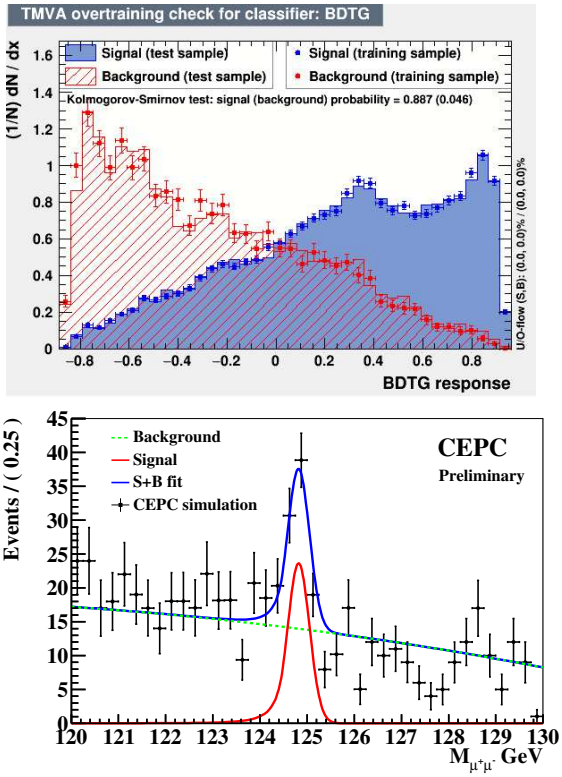

Fig. 3. (color online) The BDT response distribution (top) and the post-fit result with BDT improvement (bottom).

(∼70%). The exclusive method of the k_t algorithm for e^+e^- collisions in Fastjet [27] is used to reconstruct two jets with the particles expect the chosen μ^- and μ^+, and the jets are sorted by energy. We perform an analysis on the Z(qq̄)H(μμ) production. Apart from the previously mentioned variables related to the H(μμ) system, we further exploit the following selections on jets: the third component of di-jet system momentum $P_{Z_{jj}}$, the recoil mass of the di-jet system $M^{jj}_{\rm recoil}$ mass of jets $M_{j1,2}$, and the invariant mass of the di-jet system M_{jj}.

4.1 Cut-count analysis

A cut-count analysis is performed for the exclusive analysis. The event flow under selections are summarized in Table 2. Selections on single and di-jet masses eliminate most background without hard jets. The recoil mass cut further reduces the Z(ll)Z(qq̄) background.

As in the inclusive channel, we perform a likelihood fit to extract the signal yield and strength parameter. The quality of the fit is demonstrated in Fig. 5. The signal yield from the fit is 75.5±12.5. The signal strength can be determined with an uncertainty from -16% to 17%, at 68% confidence level. The signal significance under the peak at 124.3–125.2 GeV is found to be 10.8σ.

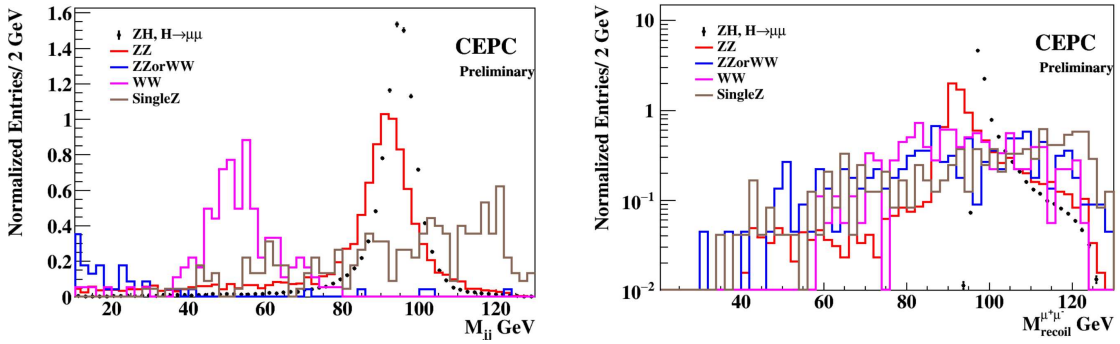

Fig. 4. (color online) Distributions of $M_{\rm recoil}^{\mu^+\mu^-}$ and M_{jj} in Z($q\bar{q}$)H($\mu^+\mu^-$) analysis. The distributions are normalized to 10.

Table 2. The cut-chain with cut-base method in the Z($q\bar{q}$)H($\mu\mu$) analysis.

category	signal	ZZ	WW	ZZ or WW	single Z	2f
Preselection	156.3	390775	183751	463361	101164	63217
$120<M_{\mu^+\mu^-}<130$	141.6	3786	181	227	244	100
$M_{j1}>4.2$ $M_{j2}>2.8$	133.0	3216	111	0	9	60
$M_{jj}>76.0$	127.5	2917	2	0	8	59
$90.9<M_{\rm recoil}^{\mu^+\mu^-}<93.5$	75.2	893	0	0	0	0
$20<P_{{\rm T}_{\mu^+\mu^-}}<64$	74.5	777	0	0	0	0
$-58<P_{{\rm Z}_{\mu^+\mu^-}}<58$	74.5	748	0	0	0	0
$\cos\theta_{\mu^+}>-0.98$ $\cos\theta_{\mu^-}<0.98$	74.2	747	0	0	0	0
efficiency	47.5%					

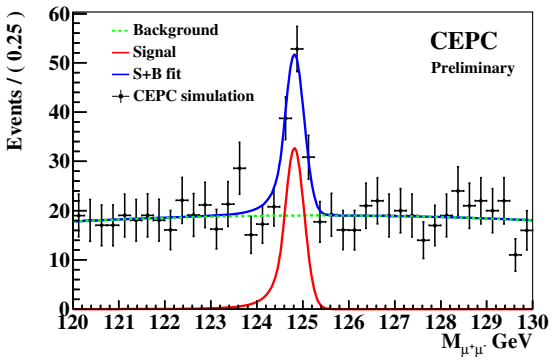

Fig. 5. (color online) The invariant mass spectrum of the di-muon system in the $Z(qq)H(\mu\mu)$ analysis. The dotted points with error bars represent the data from the CEPC simulation. The solid red and dashed green lines correspond to the signal and background contributions respectively, and the solid blue line represents the post-fit value of the total yield.

4.2 BDT improvement

In order to achieve the highest significance, we perform a two-step multivariate analysis. The first step exploits a MLP (multilayer perceptron) [26] method to suppress the fully leptonic WW and ZZ backgrounds. After applying $M_{\rm recoil}^{\mu^+\mu^-} > 90$ GeV, 4 variables including $M_{j1,2}$, M_{jj} and $M_{\rm recoil}^{jj}$ are considered as inputs for the MLP. The effectiveness of this MLP is shown in Fig. 6. After requiring the MLP response to be greater than 0.71, we exploit a BDTG to further reduce the backgrounds from semileptonic ZZ and WW. In this second step, the variables $\cos\theta_{\mu^\pm}$, $\cos\theta_{\mu^\pm {\rm Z}}$, $P_{{\rm Z}_{\mu^+\mu^-}}$, $P_{{\rm Z}_{jet12}}$, $\cos\theta_{j1/j2,H}$, $\cos\theta_{j1,2}$, and M_{jj} are taken as inputs.

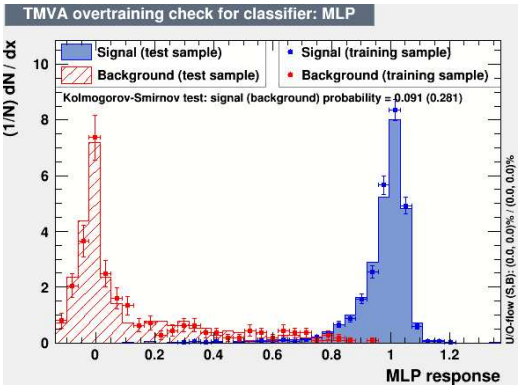

Fig. 6. (color online) The MLP result and the overtraining test in the $Z(qq)H(\mu\mu)$ analysis.

After the two-step multivariate analysis, we require a BDTG response>-0.13, $90.4 < M_{\rm recoil}^{\mu^+\mu^-} < 93$ GeV, and $28<P_{{\rm T}_{\mu^+\mu^-}}<64$ GeV. Finally, we perform a likelihood fit to extract the signal yield and strength parameter, as

shown in Fig. 7. The signal yield from the fit is 73.4±12.4. Based on a likelihood scan, the signal strength can be determined with an uncertainty from -16% to 17%, at 68% confidence level. The significance of the signal in the peak region 124.3–125.2 GeV is found to be 10.8σ, which means the best boundary to distinguish signal and background is nearly an N-dimensional rectangle in the parameter phase space.

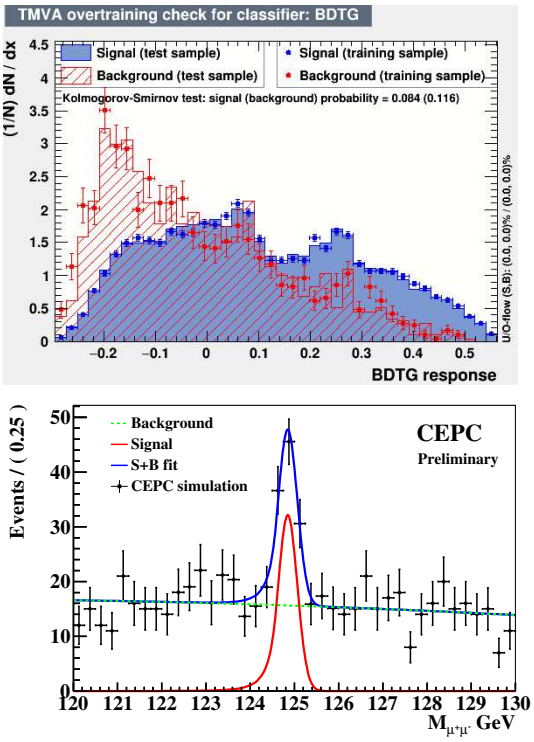

Fig. 7. (color online) The BDT response (top) and the final fit result (bottom) in the Z(qq)H($\mu\mu$) channel analysis

5 Summary

The feasibility of measuring $H\to\mu^+\mu^-$ at the CEPC has been studied considering center-of-mass energy 250 GeV collisions and 5000 fb^{-1} integrated luminosity. The measurement was performed in two complementary channels: ZH production without measuring the Z boson decay, and ZH production with the Z boson decaying hadronically. For each decay channel, a cut-count analysis was tested and followed with an improvement using multivariate techniques. Similar results are obtained from the two channels.

Finally, we want to mention in brief possible systematic factors affecting this future analysis. By referring mostly to Ref. [19], which shares most of the common factors, the systematics uncertainty should be under control, while the statistical uncertainty will dominate for this analysis at the CEPC.

Over 10 σ significance can be reached for the signal $H\to\mu^+\mu^-$ process. The accuracy of the signal strength can be measured with ±17% uncertainty and the associated H-μ-μ coupling can be restricted to 10% level. The results are comparable to the High-Luminosity LHC.

The authors would like to thank Xin Mo, Dan Yu and Yuqian Wei for useful discussions.

Appendix A

Table A1. Details of the two-fermion background samples.

process	final states	σ/fb	events expected
uu	u,$\bar{\text{u}}$	9995.35	50476527
dd	d,$\bar{\text{d}}$	9808.71	49533965
cc	c,$\bar{\text{c}}$	9974.20	50369725
ss	s,$\bar{\text{s}}$	9805.39	49517234
bb	b,$\bar{\text{b}}$	9803.04	49505372
qq	q,$\bar{\text{q}}$	49561.30	250284565
e2e2	$\mu^-\mu^+$	4967.58	25086253
e3e3	$\tau^-\tau^+$	4374.94	22093447
bhabha	e^-,e^+,γ	24992.21	126210660

Table A2. Details of the four-fermion background samples.

process	final states	σ/fb	events expected
ZZ(h)utut	up, up, up, up	83.09	419604
ZZ(h)dtdt	down, down, down, down	226.2	1142310
ZZ(h)uu_notd	uq, uq, (sq, bq), (sq, bq)	95.65	483032
ZZ(h)cc_nots	cq, cq, (dq, bq), (dq, bq)	96.04	485002
ZZ(sl)nu_up	$nu_{\mu,\tau}$,$nu_{\mu,\tau}$, up, up	81.72	412686
ZZ(sl)nu_down	$nu_{\mu,\tau}$,$nu_{\mu,\tau}$, down, down	134.86	681043

Continued on next page

Table A2. – continued from previous page

ZZ(sl)mu_up	mu, mu, up, up	82.38	416019
ZZ(sl)mu_down	mu, mu, down, down	127.96	646198
ZZ(sl)tau_up	tau, tau, up, up	39.78	200889
ZZ(sl)tau_down	tau, tau, down, down	64.3	324715
ZZ(l)4tau	τ^-,τ^+,τ^-,τ^+	4.38	22119
ZZ(l)4mu	μ^-,μ^+,μ^-,μ^+	14.57	73578
ZZ(l)taumu	τ^-,τ^+,μ^-,μ^+	17.54	88577
ZZ(l)mumu	ν_τ,$\bar{\nu}_\tau$,μ^-,μ^+	18.17	91758
ZZ(l)tautau	ν_μ,$\bar{\nu}_\mu$,τ^-,τ^+	9.2	46460
WW(h)cuxx	uq, cq, down, down	3395.48	17147189
WW(h)uubd	uq, uq, dq, bq	0.05	252
WW(h)uusb	uq, uq, sq, bq	165.94	837997
WW(h)ccbs	cq, cq, sq, bq	5.74	28987
WW(h)ccds	cq, cq, sq, dq	165.57	836128
WW(sl)muq	mu, nu, up, down	2358.69	11911394
WW(sl)tauq	tau, nu, up, down	2351.98	11877519
WW(l)ll	mu, tau, nu_μ,nu_τ	392.96	1984448
ZZorWW(h)udud	uq, uq, dq, dq	1570.4	7930514
ZZorWW(h)0cscs	cq, cq, sq, sq	1568.94	7923141
ZZorWW(l)mumu	mu, mu, nu_μ,nu_μ	214.81	1084790
ZZorWW(l)tautau	tau, tau, nu_τ,nu_τ	205.84	1039492
sZ(l)etau	e^-,e^+,τ^-,τ^+	150.14	758207
sZ(l)emu	e^-,e^+,μ^-,μ^+	852.18	4303527
sZ(l)enu	e^-,e^+,$\nu_{\mu,\tau}$,$\bar{\nu}_{\mu,\tau}$	29.62	149581
sZ(sl)eut	e,e,up,up	195.86	989093
sZ(sl)edt	e,e,down,down	128.72	650036
sZ(l)numu	ν_e,$\bar{\nu}_e$,μ^-,μ^+	43.33	218816
sZ(l)nutau	ν_e,$\bar{\nu}_e$,τ^-,τ^+	14.57	73578
sZ(sl)nu_up	ν_e,$\bar{\nu}_e$, up, up	56.09	283254
sZ(sl)nu_down	ν_e,$\bar{\nu}_e$, down, down	91.28	460964
sW(l)mu	e,nu_e,mu,$nu_{\mu,\tau}$	429.2	2167446
sW(l)tau	e,nu_e,tau,$nu_{\mu,\tau}$	429.42	2168556
sW(sl)qq	e,nu_e,up,down	2579.31	13025535
sWorsW(l)el	e^-,e^+,ν_e,$\bar{\nu}_e$	249.34	1259167

References

1 S. Chatrchyan et al (The CMS Collaboration), JHEP, **06**: 081 (2013)
2 G. Aad et al (The ATLAS Collaboration), Phys. Lett. B, **726**: 88 (2013)
3 G. Aad et al (The ATLAS Collaboration), Phys. Lett. B, **726**: 120 (2013)
4 V. Khachatryan et al (The CMS Collaboration), Eur. Phys. J. C, **75**: 212 (2015)
5 V. Khachatryan et al (The CMS Collaboration), Phys. Rev. D, **92**: 012004 (2015)
6 G. Aad et al (The ATLAS Collaboration and CMS Collaboration), Phys. Rev. Lett., **114**: 191803 (2015)
7 CEPC-SppC Preliminary Conceptual Design Report: Physics and Detector, by the CEPC Study Group
8 G. Aad et al (ATLAS Collaboration), Phys. Lett. B, **738**, 68 (2014) doi:10.1016/j.physletb.2014.09.008 [arXiv:1406.7663 [hep-ex]]
9 V. Khachatryan et al (CMS Collaboration), Phys. Lett. B, **744**, 184 (2015) doi:10.1016/j.physletb.2015.03.048 [arXiv:1410.6679 [hep-ex]]
10 M. Aaboud et al (ATLAS Collaboration), Phys. Rev. Lett., **119**: 051802 (2017)
11 (ATLAS Collaboration), ATL-PHYS-PUB-2013-014
12 (CMS Collaboration), arXiv:1307.7135 [hep-ex]
13 H. Aihara et al, arXiv:0911.0006 [physics.ins-det]
14 S. Kawada et al, arXiv:1801.07966 [hep-ex]
15 M. Faucci Giannelli and S. Celani, arXiv:1603.04718 [hep-ex]
16 W. Kilian, T. Ohl, and J. Reuter, Eur. Phys. J. C, **71**: 1742 (2011)
17 T. Sjostrand, L. Lonnblad, S. Mrenna, and P. Z. Skands, hep-ph/0308153
18 Mora de Freitas, P. and Videau, H., LC-TOOL-2003-010
19 Z. Chen, Y. Yang, M. Ruan, D. Wang, G. Li, S. Jin, and Y. Ban, Chin. Phys. C, **41**(2), 023003 (2017)
20 The ILD concept group, arXiv:1006.3396
21 T. Behnke, J. Brau, P. Burrows et al, arXiv: 1306.6329
22 H. Baer, T. Barklow, K. Fujii et al, arXiv:1306.6352
23 Manqi Ruan, arXiv: 1403.4784
24 X. Mo, G. Li, M. Q. Ruan, and X. C. Lou, Chin. Phys. C, **40**(3): 033001 (2016)
25 D. Bardina, M. Bilenkya, D. Lehnerc, A. Olchevskib, and T. Riemann, Nucl. Phys. Proc. Suppl. B, **37**: 148–157 (1994)
26 P. Speckmayer, A. Hocker, J. Stelzer, and H. Voss, J. Phys. Conf. Ser., **219**: 032057 (2010)
27 M. Cacciari, G. P. Salam, and G. Soyez, Eur. Phys. J. C, **72**: 1896 (2012) doi:10.1140/epjc/s10052-012-1896-2 [arXiv:1111.6097 [hep-ph]]
28 R. G. Lomax and D. L. Hahs-Vaughn, *Statistical concepts: a second course*, Taylor and Francis, Hoboken, NJ, 2012